Materials Science & Engineering A 662 (2016) 296–302

Contents lists available at ScienceDirect

Materials Science & Engineering A

journal homepage: www.elsevier.com/locate/msea

Sample size and orientation effects of single crystal aluminum

J.H. Wu, W.Y. Tsai, J.C. Huang*, C.H. Hsieh, Guan-Rong Huang

Department of Materials and Optoelectronic Science, National Sun Yat-Sen University, Kaohsiung 804, Taiwan ROC

ARTICLE INFO

Article history:
Received 24 November 2015
Received in revised form
14 March 2016
Accepted 16 March 2016
Available online 17 March 2016

Keywords:
Single crystal aluminum
Size effect
Tension test
Compression test
Focused ion beam

ABSTRACT

The mechanical behavior of single crystal Al sample with different sizes in mini-, micro- and nano-scales and different loading directions along [111] and [110] have been systematically investigated. The sample size and orientation effects are examined. The results are compared with previously reported data on other face-centered cubic Ni, Cu, Au and Ag, establishing an interesting trend for sample size effect with respect to stacking fault energy. With higher stacking fault energy and thus higher dislocation mobility such as Al, the sample size dependence would be lower.

1. Introduction

In recent years, the fast development of nano-technology adopts numerous materials in small scale for new devices, including sensors, actuators, and microelectronic devices. Such device sizes have been reduced down to micro- or nano-scales. The understanding of mechanical properties in micro- or nano-scales and the significance of size effects have become an essential task. The size effect, particularly, the idea of “smaller is stronger” has been explored for some nanocrystalline materials [1] and single crystals [2–5]. Deformation of miniaturized single crystals with physical dimensions in the micro to nano range typically exhibit higher flow stresses. The size effect was purposed to be a result of the reduced sample size smaller than the characteristic length for dislocation multiplication, resulting in dislocation starvation [6,7]. An increase in flow stress for reduced micropillar samples under compression was first reported by Uchic et al. [2], using the focused ion beam (FIB) technique and the nano-indenter equipped with a flat diamond tip. By using this method, the micro/nano-scaled measurements for size effects have been researched on various materials such as Au [3,4,6,8], Cu [9–11], Al [7,12], and Ni [2,13–15].

For typical face-centered cubic (FCC) Ag, Au, Cu, Ni and Al with various stacking fault energy values (∼22, ∼45, ∼78, ∼128 and ∼166 mJ/m^2, respectively) [16], it was found that when the sample size was reduced to nano-scale, the mechanical properties such as yield strength and plasticity would both increase [2,5,6,17,18,19]. This phenomenon is related to restriction of dislocation motion. There is no space to induce abundant dislocations. The extended elongation originated from lattice constant extension and nano-twinning are activated. Among all the previous reports, after normalized by shear modulus and Burger's vector [20], the stress increment with decreasing sample size does not seem to exhibit strong dependence with respect to the stacking fault energy. It is also rare to conduct size effect from the same single crystal from bulk down to nano scales, as well as the size effect for different sample orientations. Thus, in this study, the single crystal Al samples, along the [111] and [110] directions, are selected to be loaded in mini-, micro- and nano-scales. The extracted results are discussed and compared with previous findings.

2. Experiment method

Single crystal Al with the rod crystal parallel to [111], measuring 40 mm in height and 10 mm in diameter, was provided by Ames Laboratory, Iowa, USA. The purity is 99.95%. The growth orientation of this Al single crystal was investigated by X-ray diffraction (XRD, SIEMENS D5000) with Cu-K$_\alpha$ radiation. After careful mechanical grinding, polishing and electropolishing to result in lustrous and smooth surfaces, the exact crystalline orientations were determined by electron back scattering diffraction (EBSD) attached on scanning electron microscope (SEM, JSM-6330). We select two orientations, [111] and [110], for our study for the ease of sample extraction. Samples were accordingly sliced from the single crystal and, subsequently, tested in both tension and compression.

Three dimensions of the mechanical testing specimens were

---

* Corresponding author.
E-mail address: jacobc@mail.nsysu.edu.tw (J.C. Huang).

http://dx.doi.org/10.1016/j.msea.2016.03.076
0921-5093/

prepared, namely, the dog-bone shape samples for mini-tension test (in mini scale), cylindrical pillar shape samples for micro-compression (in micro scale), and specially designed dual-gage samples for nano-tension test (in nano scale), as described in details below. Multiple tests were conducted and the representative and average data are presented. Because of the difficulty (and the cost) in preparing micro-scaled tensile samples using our FIB method, we only carry out micropillar compression for the micro-scaled tests. There might be doubts if we can compare the tension results in the mini- and nano-scales with the compression results in micro-scale. The tension/compression asymmetry needs to be explored further. Yu et al. [21] have examined the yield stress σ_y asymmetry in AA1050 commercially pure Al samples with various grain sizes. For fine-grained Al samples with the average grain size of 0.35–0.75 μm, the σ_y asymmetry can be at most 20%, with the higher compression stresses. When the grain size is increased to 2.5 μm, the tension/compression asymmetry is no longer observed. In addition, the tension/compression asymmetry in Al single crystals was found to be very minor [22–24]. We thus consider the minor σ_y asymmetry (even for 0-20%) of the current Al samples for our wide-scaled comparison (for 300–1000% σ_y difference) on the size and orientation effect is logical and acceptable.

The mini-scaled samples, with tensile gauge length of 1.5 mm, width of 0.5 mm and thickness of 0.5 mm, were machined with the tensile direction parallel [111] or [110]. The mini tensile tests were conducted using the MTS Tytron-250 Microforce Testing System (minitester). The strain rate was set to be $2 \times 10^{-3}\,s^{-1}$, within the quasi static state.

The micro-scaled samples were prepared by the dual focused ion beam (FIB, Seiko, SEIKO SMI3050 SE), following the Uchic method [2]. A Ga^+ ion beam operated at 30 keV and 7–12 nA was initially directed perpendicular to the surface of the Al single crystal to mill a crater with a much larger size island located in the center. Then, the much lower currents of 0.7–0.09 nA, in avoidance from appreciable Ga^+ damage [25], were selected to refine the preserved island in the center to get a desired diameter and height of the pillar. The pillar samples have a minor taper angle less than 2°, with 4.5 ± 0.5 μm in height and $\sim 2.0 \pm 0.2$ μm in diameter. The samples were loaded in uniaxial compression by nano-indentation system MTS Nano-Indenter XP equipped with a flat-end Berkovich indenter under the displacement control mode. The strain rate was set to $7 \times 10^{-3}\,s^{-1}$, also within the quasi static state. The maximum displacement was preset to be about 320 nm.

The nano-scaled samples were also prepared by the FIB process, and also loaded by the MTS Nano-Indenter XP. The configuration of this newly designed nano-tension samples has been reported in our earlier paper [26], as shown in Fig. 1. This sample contains one central beam under compression receiving the indentation load, and two parallel gage sections under tension when the central pillar is pressed downward. The tensile gage section of this sample has a dimension of about 400 ± 100 nm in length, 200 ± 50 nm in width, and 150 ± 50 nm in thickness, maintaining a typical of gage length to width (or thickness) ratio of about 2:1. The central compressive beam is essentially a much larger and stronger pillar, which has a dimensional width over five times of the tensile gage section to ensure effective tension deformation within the tensile gage section with minimum deformation from the central beam. The nano-scaled specimens were loaded at a constant displacement rate mode 0.4 nm/s, or a strain rate about $1 \times 10^{-3}\,s^{-1}$. The maximum displacement was set to be 400 nm.

3. Results and discussion

The Al single crystal sample was characterized by XRD along the cross-sectional plane of the rod and the result is shown in Fig. 2(a). Its single peak clearly reveals the growth direction of the crystal parallel is [111]. This orientation is further confirmed by the EBSD inverse pole figures, as shown in Fig. 2(b).

Results obtained from mini-scaled tension tests are demonstrated in Fig. 3 for the [111] samples. The representative stress-strain curve is shown in Fig. 3(a), from which the Young's modulus of 70 ± 2 GPa and 0.2% offset yield strength of $\sim 60 \pm 3$ MPa are measured. It is well known that pure Al is among the most isotropic metals, with Poisson ratio of 0.362, very close to the ideal isotropic value of 0.333, plus E_{111}/E_{iso} or E_{110}/E_{iso} above 0.95 (where E_{111}, E_{110} and E_{iso} represent the modulus along the [111], [110], and theoretically calculated isotropic value based on elastic constants) [27]. The tensile elastic strain is only ~0.1% and the tensile failure elongation reaches $8 \pm 1\%$. All the related mini-scaled data are compiled in Table 1. Parallel tests were also performed on the [110] mini samples, and the tensile yield strength is $\sim 40 \pm 3$ MPa. From the SEM images of the deformed sample, the slip trace can be seen on the gauge section surface, as shown in Fig. 3(b). No twinning was observed from careful surface trace examination. The 35° marked in the figure is the angle between the tensile loading direction, [111], and the slip direction, one of the $\langle 110 \rangle$ family such as [110].

Results from the micro-scaled tests are presented in Fig. 4. The representative stress-stain curve for the [111] samples is shown in Fig. 4(a). Since the initial loading would be affected by the surface flatness of the pillar top, the elastic modulus is usually extracted from the slope of the unloading curve, which value gives about calculated by the unloading part slope of the stress-stain curve is about 72 ± 4 GPa. The micro-scaled yield strength is

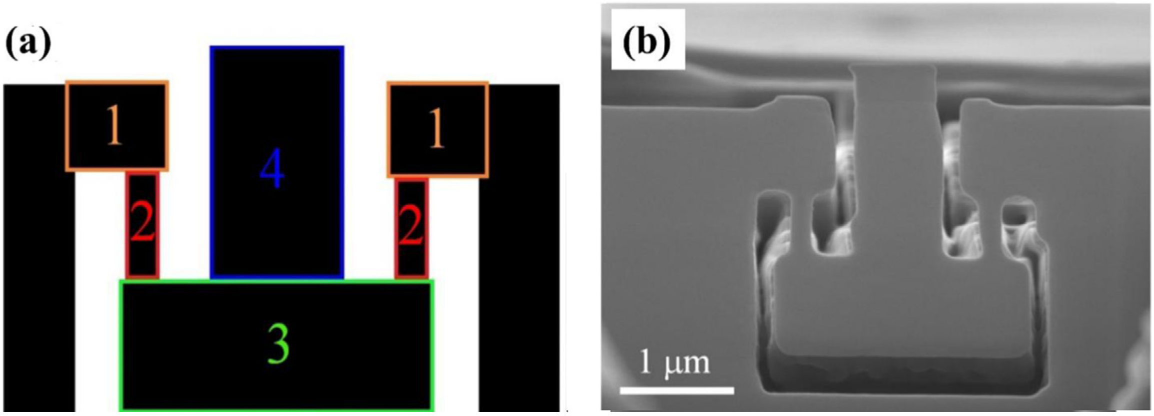

Fig. 1. Schematic drawing (a) and SEM micrograph (b) of the self-designed nano-tension specimen.

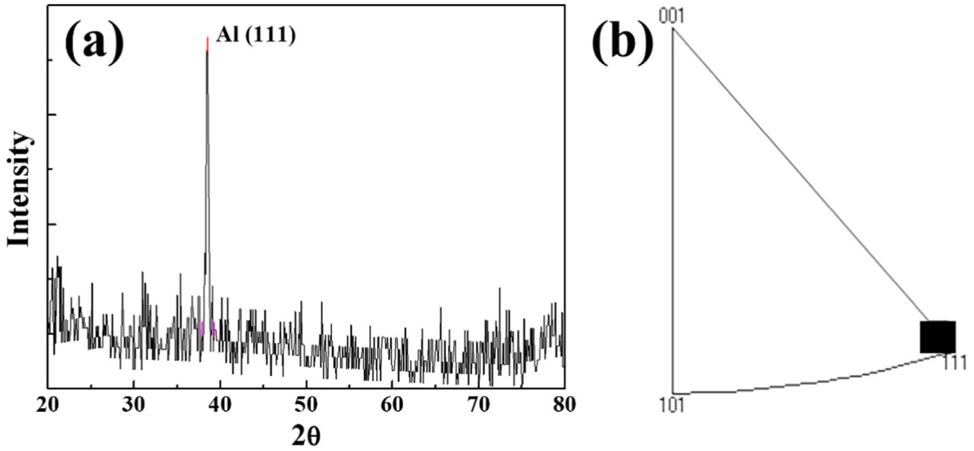

Fig. 2. (a) XRD pattern shows a sharp peak located at 2θ=38.47°. (b) Inverse pole figure measured from the cross-sectional section of the single crystal rod, i.e., from the (111) plane.

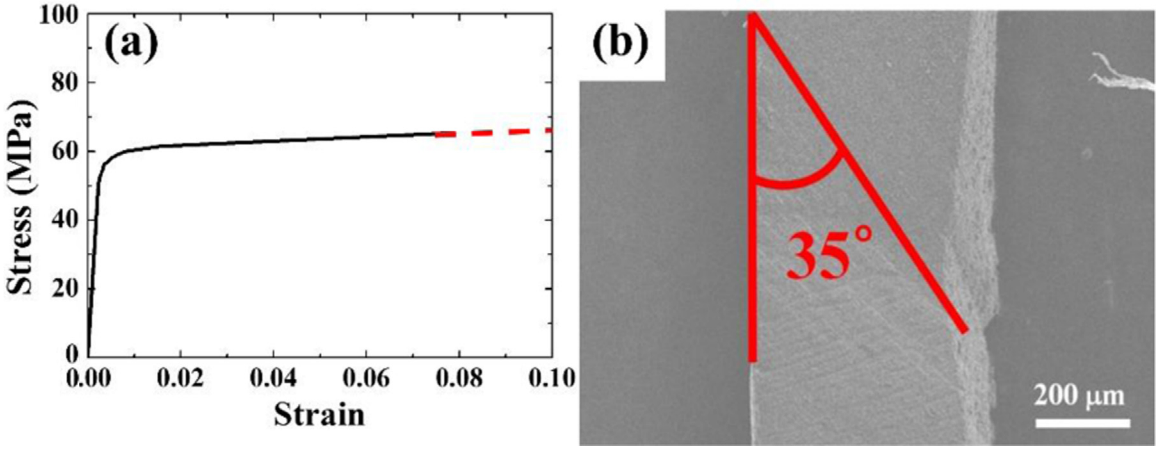

Fig. 3. (a) The representative stress-strain curve of the mini-tension [111] sample. (b) The SEM micrographs of the deformed [111] sample.

Table 1
Summary of the mechanical test results for the Al single crystal in mini, micro and nano scale along the [111] and [110] directions. The mini tension tests were stopped when the elongation is over 8% in prevention from sample touching to the strain gage.

	E (GPa)		σ_{YS} (MPa)		Elastic strain (%)		Failure strain (%)	
	[111]	[110]	[111]	[110]	[111]	[110]	[111]	[110]
Mini scale	70 ± 2	70 ± 3	60 ± 3	40 ± 3	0.1	0.1	> 8	> 8
Micro scale	72 ± 4	74 ± 4	180 ± 5	116 ± 5	0.25	0.16	–	–
Nano scale	72 ± 3	72 ± 5	750 ± 30	450 ± 10	1.0	0.6	10 ± 1	11 ± 2

~180 ± 5 MPa, much higher than the mini samples. Data from the micro-scaled samples are summarized in Table 1. The elastic strain estimated from the unloading curve is ~0.25%, consistent with the elastic strain measured from the mini samples. Micro-compressed pillar samples are shown in Fig. 4(b). From the SEM image, the dislocation slip traces are seen on the deformed sample. Again, no twin was ever seen from careful surface trace examination. The angle between the vertical edge and the slip line is measured to be about 35.5°, also consistent with the predicted angle between the loading compressive loading direction ([111]) and the slip direction (one of the ⟨110⟩ family, such as [110]), the same as the mini specimens. Again, parallel micro-scaled tests were conducted on the [110] samples. The extracted yield strength is ~116 ± 5 MPa, as presented in Fig. 4(c) and listed in Table 1. From the SEM image in Fig. 4(d) of the deformed pillar loading along [110], the measured 60° is consistent with the predicted angle between the loading compressive loading direction ([110]) and the slip direction (one of the ⟨110⟩ family, such as [101]).

The nano-scaled tensile tests were also conducted. The representative stress-strain curve for the [111] samples is presented in Fig. 5(a), the modulus calculated from the unloading part slope is also about 72 ± 3 GPa. The average tensile strength is about 750 ± 30 MPa. The elastic strain from the unloading part is about 1%, and the real failure strain cannot be measured accurately since once one of the two tensile gage sections is failed the other gage section would be inclined to the central beam, as demonstrated in the SEM image of the deformed sample in Fig. 5(b). The parallel tests were also done on the [110] nano samples. The modulus is still similar, about 72 ± 5 GPa, and the tensile stress is about 450 ± 10 MPa. All the related nano-scaled data are also compiled in Table 1.

The orientation analysis for the [111] and [110] single-crystal samples is rather straightforward, independent of the mini, micro or nano-scaled samples. Since the primary deformation

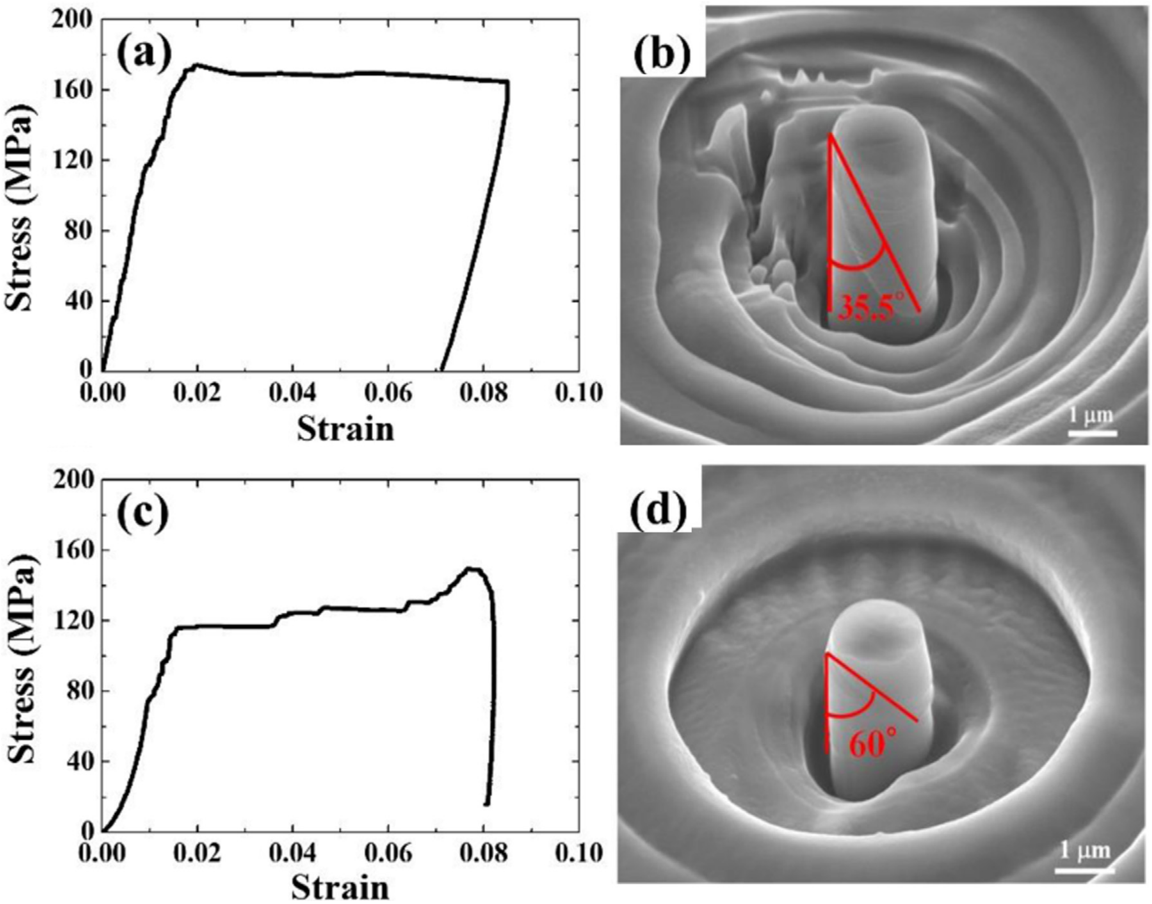

Fig. 4. The representative stress strain curves of the (a) [111] micropillar sample and (c) [110] micropillar sample. The SEM micrographs of the (b) [111] deformed sample and (d) [110] deformed sample. The elastic modulus was measured based on the unloading curves, as the initial loading part might be affected by the slightly uneven pillar top surface.

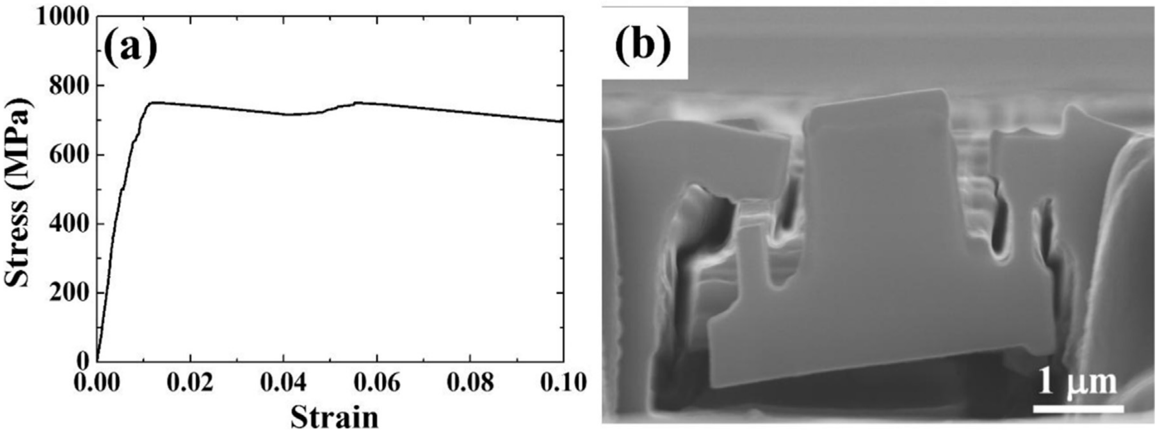

Fig. 5. (a) The representative stress-strain curve of the nano-tension [111] sample. (b) The SEM micrographs of the deformed [111] sample. When one of the tensile gage-sections is failed (in this case the left one), the whole specimen would be tilted.

mechanism in all three scaled samples is dislocation slip, no twinning, the orientation dependence can be readily calculated using the Schmid Law and the critical resolved shear stress (CRSS) ($=\sigma_{yield}$. $\cos\theta \cos\lambda$, where θ and λ are the angels between the loading axis with respect to the slip plane normal and slip direction). For example, the yield strength of the [111] micro-pillar is about 180 MPa. For all the twelve {111} ⟨110⟩ slip systems, the slip system from the CRSS calculation for aluminum single crystal sample loaded along the [111] direction was listed in Table 1. The Schmid factor can only be 0 or ± 0.27. The larger 0.27 would lead to the observed slip line, corresponding to $\theta = 35.26°$ between the loading direction [111] and the slip direction [110]. The resulting CRSS is therefore ~50 MPa (180 MPa × 0.27). The same can be calculated for the [110] sample. In this case, the Schmid factor can only be 0 or ± 0.41. The larger 0.41 would lead to the observed slip line, which corresponds to $\theta = 60°$ between the loading direction [110] and the slip direction [110]. The resulting CRSS is also ~50 MPa (116 MPa × 0.41). The extracted CRSS values are compiled in Table 1.

The stress can be expressed by the general equation,

$$\sigma = \sigma_o + K'D^{-n'}, \quad (1)$$

where the first term σ_o represents the sample size independent term, and the second terms corresponds to the sample size dependent contribution, in which D represents the sample dimension, and the K′ factor and exponent n′ can be evaluated for various FCC metals. Since σ_o is rather small for pure metals in comparison with the second term for flow stress in fine scale, it can sometimes be ignored. Thus, the size effect can be roughly simplified into

$$\sigma = K'D^{-n'}. \quad (2)$$

To apply this Eq. (2) onto the Al single crystal samples (along both the [111] and [110] directions), the resulting relationship is

$$\sigma = K'D^{-0.5637}, \quad (3)$$

where the exponent n is 0.5637. Note that we cannot find apparent difference in sample size dependence along the [111] or [110] direction, suggesting the sample size effect does not show sample orientation dependency. Since different metals have different Young's or shear moduli and lattice constants (and hence the Burger's vector), and the flow stress is a function of sample orientation, Eq. (2) can generally be expressed by the normalized shear stress, as treated before [20],

$$\frac{\tau_{CRSS}}{G}\cdot\frac{b_{Al}}{b_x} = KD^{-n}, \quad (4)$$

where τ_{CRSS} is the critical resolved shear stress, G the shear modulus along the loading direction, b_{Al} the Burger's vector of pure Al (0.234 nm), and b_x the Burger's vector of element x. The related values for Al, Ni, Cu, Au, and Ag from the current study and several references [4,6,7,9,12–14,28] are compiled in Table 2. The normalized shear stress as a function of size dimension for Al, Ni, Cu, Au and Ag is presented in Fig. 6(a). By linear square fit with ~90% or above accuracy, the negative slopes for each element can be extracted. This slope is in fact the exponent n in Eq. (4), its values being 0.5637 for Al, 0.5798 for Ni, 0.6346 for Cu, 0.7801 for Au, and 0.8652 for Ag. It is obvious there is a trend with respect to the stacking fault energy γ of each element for the micro- and nano-scale samples, as plotted in Fig. 6(b). It is apparent that the lower slope is held for elements with higher stacking fault energy. This means that Al (~166 mJ/m^2) has the lowest sample size effect, and Ag (~22 mJ/m^2) possesses the highest sample size dependence. By using the log scale for the stacking fault energy γ, the trend,

$$n = 1.93\gamma^{-0.23}, \quad (5)$$

appears to be quite consistent for these five elements, as presented in Fig. 7.

It thus needs to rationalize the size effect and stacking fault energy for these FCC metals. Al with the highest stacking fault energy is inherited with the highest perfect dislocation character and the highest dislocation mobility. It is postulated that the higher dislocation mobility would lead to easier dislocation generation and multiplication in a small-scaled and confined sample size. The mechanism of dislocation starvation would be less effective causing less severe sample size effect. For materials with low stacking fault energy, partial dislocations would induce stacking faults and deformation twins, which would dominate the mechanical response [29]. When materials like Ag and Au were subjected to compression and tension tests, the stress required for deformation twinning was reported to increase drastically with decreasing sample size [30,31]. The deformation twinning is a coherent process needing high stress and the assistance of screw dislocation poles [30,31], where the twinning steps over adjacent slip planes layer by layer to cover more deforming strain. With decreasing sample size, the process for twinning propagation became less efficient. Moreover, the dislocation slip is activated in a smaller space dimension compared to the motion by twins or stacking faults. In samples with high stacking fault energy, perfect dislocations tend to slip in a more randomly distributed manner among slip planes and are more likely to conduct cross slip in 3D space, even in refined space. This would be more difficult for metals with low stacking fault energy and extended stacking faults and deformation twins. The above joint effects would lead to the negative relationship in Eq. (5).

Table 2
Comparison of the selected normalized shear stress for various sample sizes. In this table, τ_{CRSS} is the CRSS for the sample loading along [111], [110], [131], [104], [126], [269], [100] or [123], G is the shear modulus for the {111} slip plane along the ⟨110⟩ slip direction, b_{Al} is the Burger's vector magnitude for Al, and b_x is the Burger's vector magnitude for that specific metal (Al, Ni, Cu, Ag, or Ag). More data on various sample sizes and orientations are plotted in Fig. 6(a). The Schmid factor for [111], [110], [131], [104], [126], [269], [100], [123] is 0.27, 0.41, 0.37, 0.48, 0.45, 0.48, 0.41, and 0.47, respectively.

Sample	τ_{CRSS} (MPa)	G (GPa)	b (nm)	$\tau_{CRSS}b_{Al}/Gb_x$	D (nm)	[Ref]
Al [111]	16	25.9	2.34	0.6×10^{-3}	5×10^5	This study
Al [111]	49	25.9	2.34	1.9×10^{-3}	2000	This study
Al [111]	203	25.9	2.34	7.8×10^{-3}	180	This study
Al [110]	17	25.9	2.34	0.7×10^{-3}	5×10^5	This study
Al [110]	48	25.9	2.34	1.9×10^{-3}	2000	This study
Al [110]	185	25.9	2.34	7.1×10^{-3}	180	This study
Al [110]	135	25.9	2.34	5.2×10^{-3}	840	[7]
Al [110]	164	25.9	2.34	6.3×10^{-3}	430	[7]
Al [110]	226	25.9	2.34	9.5×10^{-3}	156	[7]
Al [131]	93	25.9	2.34	3.6×10^{-3}	982	[7]
Al [131]	148	25.9	2.34	5.7×10^{-3}	715	[7]
Al [131]	185	25.9	2.34	7.1×10^{-3}	600	[7]
Al [131]	470	25.9	2.34	18.2×10^{-3}	110	[7]
Al [131]	226	25.9	2.34	9.5×10^{-3}	156	[7]
Al [104]	125	25.9	2.34	4.8×10^{-3}	1070	[12]
Al [104]	182	25.9	2.34	7.0×10^{-3}	740	[12]
Al [104]	226	25.9	2.34	8.3×10^{-3}	520	[12]
Al [104]	187	25.9	2.34	7.2×10^{-3}	450	[12]
Al [126]	126	25.9	2.34	4.9×10^{-3}	980	[12]
Al [126]	135	25.9	2.34	5.2×10^{-3}	696	[12]
Al [126]	176	25.9	2.34	6.8×10^{-3}	560	[12]
Al [126]	234	25.9	2.34	9.2×10^{-3}	444	[12]
Ni [111]	1650	78.7	2.03	6.5×10^{-3}	165	[13]
Ni [111]	1100	78.7	2.03	4.4×10^{-3}	215	[13]
Ni [111]	955	78.7	2.03	3.8×10^{-3}	400	[13]
Ni [269]	50	78.7	2.03	0.3×10^{-3}	30,000	[14]
Ni [269]	90	78.7	2.03	0.6×10^{-3}	10,000	[14]
Ni [269]	110	78.7	2.03	0.8×10^{-3}	5000	[14]
Ni [269]	150	78.7	2.03	1×10^{-3}	2500	[14]
Ni [269]	390	78.7	2.03	2.7×10^{-3}	1000	[14]
Cu [111]	1050	42.1	2.09	7.5	111	[9]
Cu [111]	920	42.1	2.09	6.6	155	[9]
Cu [111]	600	42.1	2.09	4.3	256	[9]
Cu [111]	420	42.1	2.09	3.0	500	[9]
Au [100]	675	24.7	2.36	11.1	290	[6]
Au [100]	450	24.7	2.36	7.4	310	[6]
Au [100]	400	24.7	2.36	6.6	400	[6]
Au [100]	170	24.7	2.36	2.8	580	[6]
Au [100]	90	24.7	2.36	1.5	960	[6]
Au [100]	50	24.7	2.36	0.8	7450	[6]
Au [123]	250	24.7	2.36	4.7	300	[4]
Au [123]	230	24.7	2.36	4.3	500	[4]
Au [123]	130	24.7	2.36	2.4	1000	[4]
Au [123]	50	24.7	2.36	0.9	2000	[4]
Au [123]	25	24.7	2.36	0.5	8000	[4]
Ag [100]	900	26.6	2.36	13.7	150	[27]
Ag [100]	750	26.6	2.36	11.4	545	[27]
Ag [100]	400	26.6	2.36	6.1	760	[27]
Ag [100]	150	26.6	2.36	2.3	1280	[27]
Ag [100]	100	26.6	2.36	1.5	2280	[27]

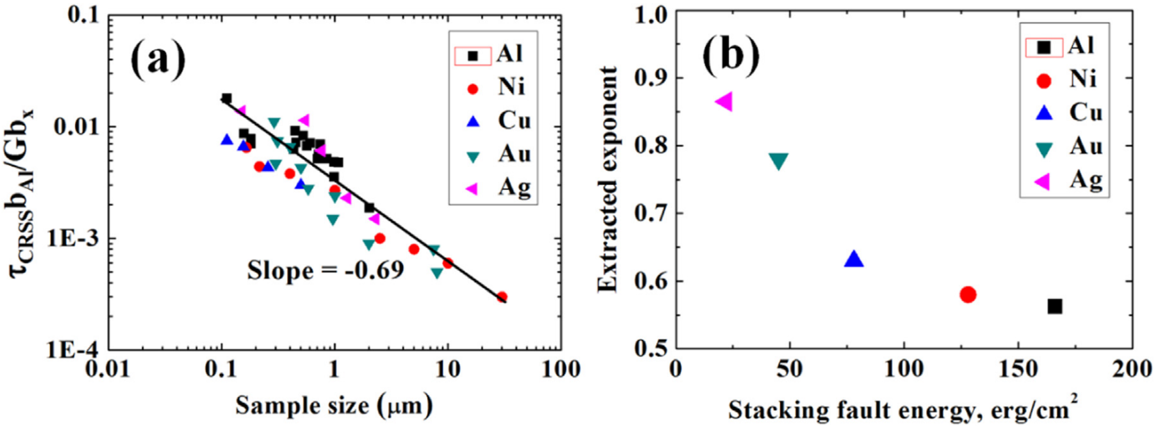

Fig. 6. (a) Comparison of the normalized shear stress as a function of size dimension for the Al, Ni, Cu, Au and Ag samples. The exponent n in Eq. (4) is the negative slopes of each fitted line for each element. (b) The extracted exponent n is plotted as a function of stacking fault energy.

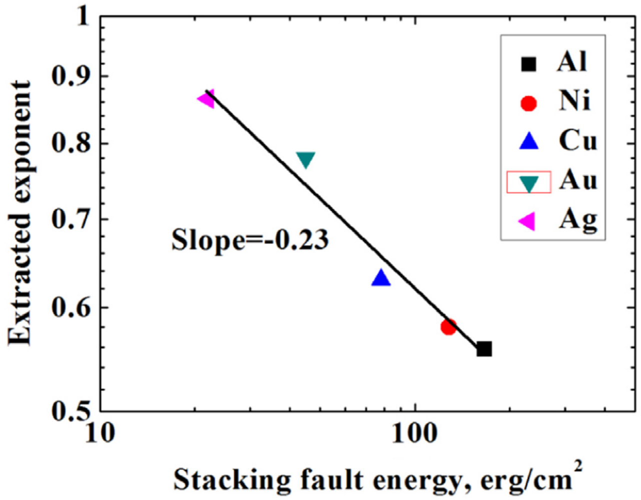

Fig. 7. The variation of extracted exponent (n) as a function of stacking fault energy for various FCC pure metals.

4. Conclusions

Based on the systematically mechanical measurements on single crystal Al sample with different sizes in mini, micron and nano scales and different loading directions along [111] and [110], the following conclusions can be drawn.

(1) The orientation dependence of Al single crystal, even in micron and nano scales, still follows well with the Schmid factor relationship and the extracted critical resolved shear stress.

(2) We cannot find apparent difference in sample size dependence along the [111] or [110] direction, suggesting the sample size effect does not show strong sample orientation dependency between these two directions.

(3) The sample size dependence of Al single crystal is compared with that of other FCC pure metals such as Ni, Cu, Au and Ag. The stacking fault energy for these metals varies from ~166 mJ/m^2 (for Al) down to ~22 mJ/m^2 (for Ag). There is a clear trend that with a higher stacking fault energy and thus higher dislocation mobility such as Al, the sample size dependence would be lower.

(4) For different samples, the power index n as a function of the stacking fault energy γ follows the power law as $n = 1.93\gamma^{-0.23}$, where n increases with decreasing γ. For Al with the highest γ, deformation is mainly driven by slip of perfect dislocations, which tend to slip in a more randomly distributed manner among slip planes and are more likely to conduct cross slip in 3D space, even in refined space. This would be more difficult for metals with low stacking fault energy and extended stacking faults and deformation twins. The above joint effects would lead to the negative relationship between sample size exponent n and stacking fault energy γ.

Acknowledgements

The authors gratefully acknowledge the sponsorship from Ministry of Science and Technology of Taiwan, ROC, under the project No. MOST 103-2120 – M-110-004. The Al crystal was provided by Prof. T. G. Nieh in University of Tennessee. Thanks are also due to Prof. Nieh for stimulating discussion and suggestions.

References

[1] K.S. Kumar, H. Van Swygenhoven, S. Suresh, Acta Mater. 51 (2003) 5743–5774.
[2] M.D. Uchic, D.M. Dimiduk, J.N. Florando, W.D. Nix, Science 305 (2004) 986–989.
[3] J.R. Greer, W.C. Oliver, W.D. Nix, Acta Mater. 53 (2005) 1821–1830.
[4] C.A. Volkert, E.T. Lilleodden, Philos. Mag. 86 (2006) 5567–5579.
[5] D. Kiener, W. Grosinger, G. Dehm, R. Pippan, Acta Mater. 56 (2008) 580–592.
[6] J.R. Greer, W.D. Nix, Phys. Rev. B 73 (2006) 245410.
[7] Z.J. Wang, Q.J. Li, Z.W. Shan, J. Li, J. Sun, E. Ma, Appl. Phys. Lett. 100 (2012) 071906.
[8] A.S. Budiman, S.M. Han, J.R. Greer, N. Tamura, J.R. Patel, W.D. Nix, Acta Mater. 56 (2008) 602–608.
[9] A.T. Jennings, M.J. Burek, J.R. Greer, Phys. Rev. Lett. 104 (2010) 135503.
[10] D. Kiener, C. Motz, T. Schöberl, M. Jenko, G. Dehm, Adv. Eng. Mater. 8 (2006) 1119–1125.
[11] R. Maaß, S. Van Petegem, D. Grolimund, H. Van Swygenhoven, D. Kiener, G. Dehm, Appl. Phys. Lett. 92 (2008) 071905.
[12] A. Kunz, S. Pathak, J.R. Greer, Acta Mater. 59 (2011) 4416–4424.
[13] C.P. Frick, B.G. Clark, S. Orso, A.S. Schneider, E. Arzt, Mater. Sci. Eng.: A 489 (2008) 319–329.
[14] D.M. Dimiduk, M.D. Uchic, T.A. Parthasarathy, Acta Mater. 53 (2005) 4065–4077.
[15] Z.W. Shan, R.K. Mishra, S.A.S. Asif, O.L. Warren, A.M. Minor, Nat. Mater. 7 (2008) 115–119.
[16] L.E. Murr, Interfacial Phenomena in Metals and Alloys, 1975.
[17] S.W. Lee, W.D. Nix, Philos. Mag. 92 (2012) 1238–1260.
[18] D.S. Balint, V.S. Deshpande, A. Needleman, E. Van der Giessen, Model. Simul. Mater. Sci. Eng. 14 (2006) 409.
[19] J.R. Greer, J.T.M. De Hosson, Prog. Mater. Sci. 56 (2011) 654–724.
[20] M.D. Uchic, P.A. Shade, D.M. Dimiduk, Annu. Rev. Mater. Res. 39 (2009) 361–386.
[21] C.Y. Yu, P.L. Sun, P.W. Kao, C.P. Chang, Scr. Mater. 52 (2005) 359–363.
[22] S.N. Buckley, K.M. Entwistle, Acta Metall. 4 (1956) 352–361.
[23] D.J. Lloyd, Acta Metall. 25 (1977) 459–466.
[24] S. Cheng, J.A. Spencer, W.W. Milligan, Acta Mater. 51 (2003) 4505–4518.
[25] D. Kiener, C. Motz, M. Rester, M. Jenko, G. Dehm, Mater. Sci. Eng.: A 459 (2007)

262–272.
[26] S.Y. Kuan, J.C. Huang, Y.H. Chen, C.H. Chang, C.H. Hsieh, J.H. Wang, Y.C. Nian, S. P. Ju, T.G. Nieh, S.H. Chen, Mater. Sci. Eng.: A 646 (2015) 135–144.
[27] A.J. Ardell, Metall. Trans. A 16 (1985) 2131–2165.
[28] S. Buzzi, M. Dietiker, K. Kunze, R. Spolenak, J.F. Löffler, Philos. Mag. 89 (2009) 869–884.
[29] J.W. Christian, S. Mahajan, Prog. Mater. Sci. 39 (1995) 1–157.
[30] S.G. Song, G.T. Gray III, Philos. Mag. A 71 (1995) 661–670.
[31] M. Niewczas, G. Saada, Philos. Mag. A 82 (2002) 167–191.